

# Echo-E<sup>3</sup>Net: Efficient Endo-Epi Spatio-Temporal Network for Ejection Fraction Estimation

Moein Heidari<sup>1</sup>, Afshin Bozorgpour<sup>2</sup>, AmirHossein Zarif-Fakharnia<sup>3</sup>, Dorit Merhof<sup>2</sup>, and Ilker Hacihaliloglu<sup>4,5</sup>

<sup>1</sup> School of Biomedical Engineering, University of British Columbia, Vancouver, BC, Canada

<sup>2</sup> Faculty of Informatics and Data Science, University of Regensburg, Regensburg, Germany

<sup>3</sup> School of Electrical Engineering, Iran University of Science and Technology, Tehran, Iran

<sup>4</sup> Department of Radiology, University of British Columbia, Vancouver, BC, Canada

<sup>5</sup> Department of Medicine, University of British Columbia, Vancouver, BC, Canada  
moein.heidari@ubc.ca

**Abstract.** Left ventricular ejection fraction (LVEF) is a critical metric for assessing cardiac function, widely used in diagnosing heart failure and guiding clinical decisions. Despite its importance, conventional LVEF estimation remains time-consuming and operator-dependent. Recent deep learning advancements have enhanced automation, yet many existing models are computationally demanding, hindering their feasibility for real-time clinical applications. Additionally, the interplay between spatial and temporal features is crucial for accurate estimation but is often overlooked. In this work, we propose Echo-E<sup>3</sup>Net, an efficient Endo-Epi spatio-temporal network tailored for LVEF estimation. Our method introduces the Endo-Epi Cardial Border Detector (E<sup>2</sup>CBD) module, which enhances feature extraction by leveraging spatial and temporal landmark cues. Complementing this, the Endo-Epi Feature Aggregator (E<sup>2</sup>FA) distills statistical descriptors from backbone feature maps, refining the final EF prediction. These modules, along with a multi-component loss function tailored to align with the clinical definition of EF, collectively enhance spatial-temporal representation learning, ensuring robust and efficient EF estimation. We evaluate Echo-E<sup>3</sup>Net on the EchoNet-Dynamic dataset, achieving a RMSE of 5.15 and an R<sup>2</sup> score of 0.82, setting a new benchmark in efficiency with 6.8 million parameters and only 8.49G Flops. Our model operates without pre-training, data augmentation, or ensemble methods, making it well-suited for real-time point-of-care ultrasound (PoCUS) applications. Our Code is publicly available on [GitHub](#).

**Keywords:** Echocardiography · Ejection fraction · Ultrasound.

## 1 Introduction

Left ventricular ejection fraction (LVEF) is one of the most critical indicators of cardiac function, used to assess heart failure and guide clinical decision-making

[11,14,12,21,8]. LVEF is traditionally estimated using Simpson’s biplane method on two-dimensional (2D) echocardiographic images, which requires manual segmentation of the left ventricle across multiple cardiac phases [14]. However, this process is subject to high inter-observer variability and is time-intensive [20,9]. To overcome these limitations, recent advancements in deep learning approaches have led to substantial improvements in the accuracy and robustness of EF estimation [12,11,8]. Several novel methods have been suggested to estimate EF [21], such as segmentation-based techniques [16,2], directly predict EF at the video level [16,7,13], utilize graphs and keypoints to guide the process [11,22], and employ attention mechanisms to improve performance [10]. However, these methods often suffer from common drawbacks that hinders their applicability: ① maintaining high accuracy while reducing computational overhead, making it ideal for deployment on mobile ultrasound devices and Point-of-care ultrasound (POCUS) applications [23]. PoCUS is gaining traction for bedside cardiac evaluation, offering portability, affordability, and rapid diagnostics [4]. However, LVEF estimation remains challenging due to operator variability and suboptimal image quality [15]. Crucially, automation of clinical measurements such as EF, entails efficient models to be adopted broadly in clinical settings [5]. ② These approaches often lack anatomical consistency, making them susceptible to errors in cases of image degradation, missing frames, or variability in cardiac cycles. To mitigate these problems, in this paper, we propose an efficient architecture for EF estimation where instead of treating EF estimation as a pure regression task, we explicitly incorporate anatomical prior by localizing LV contour, ensuring physiologically meaningful predictions. Specifically, we introduce the Endo-Epi Cardial Border Detector ( $E^2CBD$ ) module, along with a light-weight backbone network in our architecture which learns spatial landmarks corresponding to the LV boundaries, effectively capturing the dynamic motion of the ventricle across cardiac cycles. **Contributions.** We propose a lightweight yet effective framework that leverages endocardial and epicardial boundary features, integrating spatial and temporal dynamics through our specialized  $E^3CBD$  and  $E^3FA$  modules. Our framework incorporates anatomical priors by precisely detecting cardiac borders while extracting rich statistical features from multi-scale representations by leveraging a compound loss function specifically designed to align with the clinical definition of ejection fraction (Simpson’s method). Echo- $E^3Net$  achieves state-of-the-art (SOTA) performance with significantly fewer parameters ( $< 7M$ ) and lower computational complexity, making it suitable for real-time POCUS applications without the need for pre-training or extensive data augmentation.

## 2 Related Works

Automated LVEF estimation from echocardiographic images has long been studied, with traditional methods relying on rule-based techniques and manual left ventricle segmentation, leading to notable inter-observer variability [15]. Owing to the surge of deep learning techniques, recent advancements in convolutional

neural networks (CNNs), graph neural networks (GNNs), and transformer-based architectures have significantly enhanced the accuracy and efficiency of LVEF prediction [14]. In this regard, EchoNet-Dynamic leveraged CNNs to extract spatial features from echocardiographic video sequences and achieved SOTA accuracy in LVEF estimation [16]. Graph-based approaches, such as EchoGNN [11] and EchoGraphs [22], have demonstrated promising results by leveraging key point-based structural representations of the left ventricle. These methods improve interpretability by providing explicit shape constraints while reducing reliance on dense image-based CNN architectures [24,3]. However, a notable drawback of these approaches is that they assign smaller weights to ED and ES frames, which are clinically crucial for estimating ejection fraction, thereby diverging from standard clinical practices. To address data imbalance in LVEF regression tasks, EchoMEN [8] was proposed as a multi-expert network that dynamically weights different prediction models to optimize performance across a diverse dataset, but its reliance on multiple expert models increases computational overhead. EchoNarrator [21] employs a GCN framework to not only predict LVEF but also generate human-interpretable text explanations of the results [24]. Recently, Yang et al. [25] propose a reconstruction-based framework that leverages prior cardiac knowledge to capture local structural and motion anomalies in echocardiogram videos, while CoReEcho [9] estimates from 2D+time echocardiograms by focusing on continuous representation learning.

Unlike previous methods, our approach is designed to avoid computational intensity which makes them unsuitable for practical use in PoCUS settings. Moreover, our work uniquely integrates anatomical guidance by explicitly modeling endocardial and epicardial boundaries, as opposed to direct feature extraction from echocardiographic sequences. Lastly, we introduce a multi-component loss function tailored to align with the clinical definition of ejection fraction, ensuring a more robust and clinically meaningful estimation process.

### 3 Methodology

Given an echocardiography dataset  $\mathcal{D} := \{V^n, y^n\}_{n=1}^N$ , where each video  $V^n \in \mathbb{R}^{C \times F^n \times H \times W}$  consists of  $F^n \in \mathbb{Z}^+$  frames with spatial dimensions  $H \times W$ , and an associated EF value  $y^n \in (0, 100)$ . Here,  $N$  represents the total number of samples. Our objective is to develop a deep learning model that accurately estimates the EF value  $\hat{y}^n$  given an input echocardiogram  $V^n$ . The main pipeline of our method is illustrated in fig. 1, which mainly consists of three parts: a backbone networks, a cardiac border detector (**E<sup>2</sup>CB**) and an Endo-Epi feature aggregator (**E<sup>2</sup>FA**) module. We elaborate on each module in subsequent sections.

**Backbone Network** We highlight the importance of backbone feature extraction, emphasizing both spatial and channel-wise processing for comprehensive representation learning. Our feature extractor is derived from the encoder of LHUNet [18], leveraging convolutional modules and hybrid attention to capture

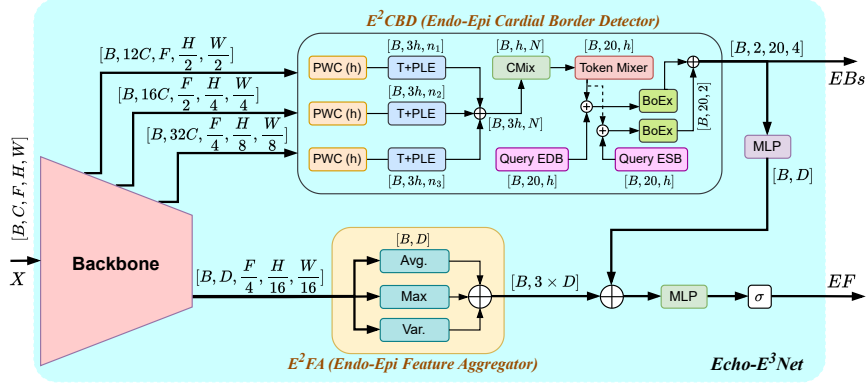


**Fig. 1.** The architecture of Echo-E<sup>3</sup>Net. Input videos first undergo feature extraction through the backbone network. The extracted features are then processed by the E<sup>2</sup>CBD module for boundary localization and the E<sup>2</sup>FA for feature aggregation.

fine-grained local details and global context efficiently. The architecture is structured into three progressive stages. It begins with an initialization block using point-wise convolution (PW-Conv) to reshape input channels for optimal compatibility. Next, pure CNN blocks extract fine-grained local features at high and mid-frequency levels, downsampling spatial dimensions while preserving critical information. The final stage integrates hybrid blocks with large-kernel spatial attention modules to capture broader spatial relationships. Unlike LHUNet, which employs deformable convolutions for segmentation, we use large static kernels for efficiency while maintaining a wide receptive field. Additionally, deep-layer channel-wise ViT attention models inter-channel dependencies, refining semantic representations. The fusion of convolutional and attention mechanisms effectively aggregates contextual information, enhancing local-global feature extraction.

**Endo-Epi Cardial Border Detector (E<sup>2</sup>CBD).** Motivated by the clinical definition of LVEF which relies on measuring the inner dimensions of the left ventricle and estimating the myocardial mass at both ES and ED phases, we introduce a landmark detection module to produce coordinates of the LV boundary location. We utilize feature-enhanced skip connections from the backbone, establishing seamless integration with our module via point-wise convolutions of channel size  $h$  to harmonize the channel dimensions, thereby facilitating direct combination in the spatial domain. To preserve the spatio-temporal structure, we incorporate learnable position embeddings, including a spatial embedding  $p_s \in \mathbb{R}^{(hw+1) \times C}$ , temporal embedding  $p_t \in \mathbb{R}^{t \times C}$  and level embedding (corresponding to different levels of skip-connection each with size  $n_i$ ,  $\forall i \in \{1, 2, 3\}$ )(T+PLE), which effectively refine spatial and temporal representations. The generated tokens are processed through a mixing operation (channel mixing: CMix) and treated as keys (Token Mixer), enabling them to

attend to query vectors derived from ED and ES frame boundaries (Query EDB, Query ESB). The interaction between these query-key representations serves as an auxiliary supervision signal, reinforcing landmark detection through border extractor module (BoEx) to precisely compute border coordinates of ES/ED frames. After extracting these boundaries, we utilize coordinate information as a spatial supervisory signal to enhance the global features obtained from the backbone, thereby refining EF estimation through additional loss functions, as detailed in section 3.1.

**Endo-Epi Feature Aggregator Module (E<sup>2</sup>FA).** To effectively leverage spatial features from the backbone network, we introduce a module that extracts statistical descriptors, enriching spatial representation for enhanced EF estimation. Specifically, E<sup>2</sup>FA computes three statistical features: **maximum**, **average**, and **variance**,  $\mathbf{F}_{stat} = \text{Concat}(\text{Avg}(\mathbf{F}_b), \text{Max}(\mathbf{F}_b), \text{Var}(\mathbf{F}_b))$ , where  $\mathbf{F}_b \in \mathbb{R}^{B \times D_b \times H_b \times W_b}$  represents the backbone feature maps. The extracted features are then concatenated with the landmark-based representations from the E<sup>2</sup>CBD module, forming  $\mathbf{F}_{final} = \text{Concat}(\mathbf{F}_{stat}, \mathbf{F}_{CBD})$ . This enriched representation is passed through an MLP, followed by a sigmoid activation  $\sigma(\cdot)$ . The final EF estimate is computed as  $EF = \sigma(\text{MLP}(\mathbf{F}_{final})) \times 100$ , ensuring the prediction aligns with the dataset’s (0, 100) scale. Integrating statistical information, E<sup>2</sup>FA enhances feature representation, complementing E<sup>2</sup>CBD’s landmark-driven approach for accurate EF estimation.

### 3.1 Loss Functions.

To ensure robust supervision for EF estimation, we define a multi-component loss function that captures key structural and functional properties of the LV. Inspired by the EF definition, we incorporate explicit supervision on ED and ES contours (EDV,ESV), as well as landmark-based border estimations to ensure accurate spatial and volumetric consistency. The *landmark loss* is used to minimize the mean squared error (MSE) between the predicted and ground truth landmarks in ED and ES frames, defined as  $\mathcal{L}_{\text{landmark}} = \text{MSE}(b_{edv}^{pd}, b_{edv}^{gt}) + \text{MSE}(b_{esv}^{pd}, b_{esv}^{gt})$ , where  $b_{edv}$  and  $b_{esv}$  represent the border positions at ED and ES phases, respectively. To ensure accurate EF estimation, the *EF loss*, calculates  $\mathcal{L}_{\text{EF}} = \text{MSE}(EF^{pd}, EF^{gt})$ , where  $EF^{pd}$  and  $EF^{gt}$  are the predicted and ground truth EF values. A *point distance loss* is incorporated to refine landmark localization by minimizing the positional error between predicted and ground-truth landmarks:  $\mathcal{L}_{\text{point}} = \frac{1}{N} \sum_{i=1}^N \|p_i^{pd} - p_i^{gt}\|^2$ , where  $p_i$  represents individual landmark positions. To further ensure anatomical consistency, we introduce the *A4C diameter loss*, which penalizes discrepancies in the predicted endocardial and epicardial border distances along the long axis of the LV in the apical four-chamber (A4C) view. This loss is formulated as:  $\mathcal{L}_{\text{diameter}} = \text{MSE}(d_{edv}^{pd}, d_{edv}^{gt}) + \text{MSE}(d_{esv}^{pd}, d_{esv}^{gt})$ , where  $d_{edv}$  and  $d_{esv}$  represent the measured LV diameters in the ED and ES frames, respectively. Additionally, the *disk height consistency loss* is introduced to maintain structural consistency between sequential cross-sectional measurements of the LV. We define it as:  $\mathcal{L}_{\text{height}} = \text{MSE}(\Delta h_{gt}, \Delta h_{pd})$ ,

where  $\Delta h$  denotes the difference between consecutive disk heights computed from the predicted and ground truth border positions along the LV length, ensuring smooth spatial transitions and realistic anatomical relationships. The final total loss function is formulated as a weighted sum of all the above loss terms:

$$\mathcal{L}_{\text{total}} = \lambda_1 \mathcal{L}_{\text{landmark}} + \lambda_2 \mathcal{L}_{\text{EF}} + \lambda_3 \mathcal{L}_{\text{point}} + \lambda_4 \mathcal{L}_{\text{diameter}} + \lambda_5 \mathcal{L}_{\text{height}} \quad (1)$$

Here,  $\lambda_i$  are weighting factors selected to keep loss values within the same range, balancing each component’s contribution to ensure accurate EF prediction while preserving anatomical coherence through clinically interpretable LV boundary constraints.

## 4 Experiments

**Dataset and Evaluation Metrics.** We utilize the **EchoNet-Dynamic** dataset [16], comprising 10,030 A4C echocardiography videos collected from Stanford University Hospital between 2016 and 2018. Each video consists of  $112 \times 112$  grayscale image sequences, annotated with 40 left ventricular (LV) contour points, along with one basal and apex point at both end-diastolic (ED) and end-systolic (ES) frames, and the corresponding ejection fraction (EF). We adopt the standard training, validation, and test splits provided by EchoNet for benchmarking. We evaluate model performance using mean absolute error (MAE), root mean squared error (RMSE), and R-squared ( $R^2$ ) as primary metrics. Additionally, we compare floating point operations (FLOPs) and model parameter counts in million (Params (M)) across different architectures to provide a comprehensive assessment of computational efficiency. **Experimental Setup.** Deep learning models typically require a fixed frame count per video scan, while EchoNet-Dynamic videos contain varying cardiac cycle lengths (20–30 frames). To handle this variability, we employ adaptive frame sampling, where during training, an initial frame index  $k$  is uniformly sampled from  $[1, F_{\text{max}}^n - F_{\text{sel}}]$ , where  $F_{\text{max}}^n$  represents the total number of frames in echocardiography video  $n$  and use  $F_{\text{sel}}$  samples starting from  $k$  [11]. Following prior work [13,16], we set  $F_{\text{sel}} = 64$  frames with a sampling frequency of 2. Unlike prior work [13,11], for shorter videos where  $F_{\text{max}}^n < F_{\text{sel}}$ , we fill missing frames using the average of previous frames rather than zero-padding, as this approach better preserves temporal consistency. Our model was trained for 45 epochs on an NVIDIA RTX 4070 GPU, equipped with 12GB memory using a batch size of 8 which took 2.5 hours, much less than similar works [21]. We employ AdamW as optimizer, setting the learning rate and weight decay to  $1e-4$ . A notable advantage of our approach over prior work is its ability to achieve high performance without relying on pretraining, data augmentation or ensemble models. In contrast, all existing methods incorporate either of them. For instance, [11] utilizes ES and ED classification as a pretraining step, while [13] leverages pretrained models from the vision domain. Our method eliminates these dependencies, demonstrating effective learning without additional supervision.

**Table 1.** Comparison of different EF estimation models on the EchoNet-Dynamic dataset. The abbreviations **R.** and **M.** correspond to the *Random* and *Mirroring* sampling strategies introduced in [17]. The EchoNet-Dynamic model is evaluated in two configurations: **(1)** estimating left ventricular ejection fraction (LVEF) at the clip level using 32 frames, and **(2)** incorporating segmentation alongside clip-level predictions to generate beat-to-beat LVEF estimates across the full video sequence. The parameter count is expressed in millions. **Blue**, and **Red** colors show best and second best.

Model	Frames	FLOPs	Params	MAE ↓	RMSE ↓	R <sup>2</sup> ↑
UVT R. [17]	128	130.00G	-	6.77	8.70	0.48
UVT M. [17]	128	130.00G	-	5.95	8.38	0.52
R3D [16]	32	92.273G	-	4.22	5.62	0.79
MC3 [16]	32	97.656G	-	4.45	5.68	0.76
EchoGNN [11]	64	-	<b>1.7</b>	4.54	-	0.77
EchoNet-Dynamic [16] (1)	32	91.974G	32	4.22	5.56	0.79
EchoNet-Dynamic [16] (2)	beat-to-beat	-	32	4.05	5.32	0.81
EchoCoTr-B [13]	36	44.907G	21	3.98	5.34	<b>0.81</b>
EchoCoTr-S [13]	36	<b>19.611G</b>	-	3.95	5.17	0.82
CoReEcho [9]	36	58.92G	21	<b>3.90</b>	<b>5.13</b>	0.82
CardiacNet [25]	16	7949G	28	<b>3.83</b>	-	-
<b>Echo-E<sup>3</sup>Net (Ours)</b>	64	<b>8.49G</b>	<b>6.8</b>	3.95	<b>5.15</b>	<b>0.82</b>

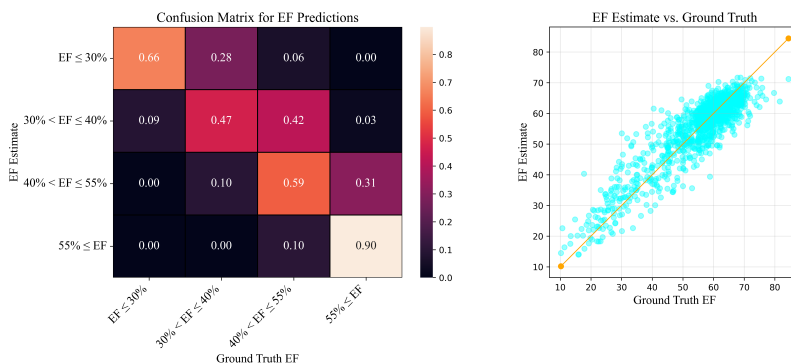


**Fig. 2.** (Left) The confusion matrix of our top-performing model. (Right) The scatter plot of our model’s EF predictions with the actual values.

## 5 Results

We evaluate Echo-E<sup>3</sup>Net against recent EF regression baselines as shown in table 1. For a fair comparison, we utilize each method’s original configuration to maintain consistency with reported results. The quantitative evaluation, presented in table 1, demonstrates that Echo-E<sup>3</sup>Net achieves either on par or SOTA performance, trained on only 64 frames, surpassing prior methods across multiple evaluation metrics, highlighting its effectiveness in EF estimation. These results are obtained while achieving substantially higher computational and memory efficiency, utilizing much fewer parameters and FLOPs compared to baselines. Specifically, while achieving competing results with CoReEcho [9] and CardiacNet [25], Echo-E<sup>3</sup>Net operates with just 8.49G FLOPs, reducing compute by

85.6% vs. CoReEcho (58.92G) and 99.9% vs. CardiacNet (7949G). Moreover, it requires only 6.8M parameters, making it 67.6% and 75.7% more compact than CoReEcho and CardiacNet, respectively, indicating that Echo-E<sup>3</sup>Net demonstrates potential for deployment in POCUS environments, where computational resources are constrained. Figure 2 presents the confusion matrix of our best-performing model, highlighting EF categories associated with heart failure risk. The scatter plot demonstrates the alignment between predicted and actual EF values. The training set of EchoNet-Dynamic exhibits an imbalanced distribution, with only 12.7% of samples having an EF ratio below 40%. However, from a clinical perspective, identifying these patients is crucial for timely intervention [6,11,1]. Notably, our model achieves superior performance for EF

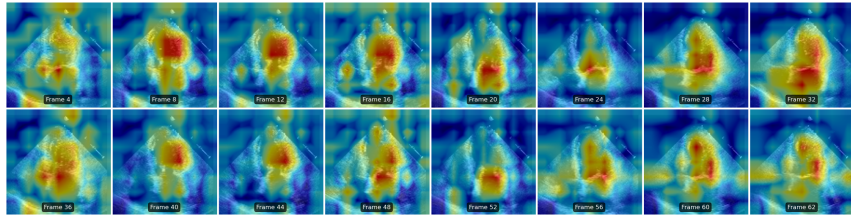


**Fig. 3.** Grad-CAM [19]. Echo-E<sup>3</sup>Net demonstrates reduced attention to background while enhancing focus on the LV, attributed to the effectiveness of the boundary detection module.

$30\% \leq EF \leq 40\%$ , a critical range requiring medical supervision, surpassing prior SOTA [11]. Additionally, Echo-E<sup>3</sup>Net’s regression slope is closer to 1, indicating a strong fit. Lastly, table 2 presents the effect of ablating individual components of Echo-E<sup>3</sup>Net. Each removal leads to a degradation in performance, reflected by increased MAE and RMSE and decreased  $R^2$  while incorporating all components achieves the optimal results. This is further illustrated in fig. 3, where our model concentrates its attention on the LV boundaries.

**Table 2.** Ablation study assessing the contribution of the E<sup>2</sup>CBD and E<sup>2</sup>FA modules in Echo-E<sup>3</sup>Net.

Model Configuration	MAE ↓	RMSE ↓	R <sup>2</sup> ↑	Params (M)
W/o E <sup>2</sup> CBD (Landmark-based)	4.11	5.38	0.78	<b>1.7</b>
W/o E <sup>2</sup> FA (Feature aggregation)	4.05	5.23	0.80	6.8
<b>Echo-E<sup>3</sup>Net (E<sup>2</sup>CBD + E<sup>2</sup>FA)</b>	<b>3.95</b>	<b>5.15</b>	<b>0.82</b>	6.8

## 6 Conclusion

We propose Echo-E<sup>3</sup>Net, a novel framework for echocardiography video EF estimation. Our network utilizes a lightweight hybrid backbone that incorporates spatial, channel attention for fine-grained feature refinement. Subsequently, inspired by the clinical workflow for LVEF estimation (Simpson’s method), we propose a landmark detection module that generates LV boundary coordinates, which are then used to guide the EF estimation task through the proposed loss function by leveraging the extracted boundaries. Echo-E<sup>3</sup>Net is highly efficient in terms of parameters and FLOPs, making it well-suited for deployment in resource-constrained PoCUS settings.

## ACKNOWLEDGMENTS

This work was supported by the Canadian Foundation for Innovation-John R. Evans Leaders Fund (CFI-JELF) program grant number 42816. Mitacs Accelerate program grant number AWD024298-IT33280. We also acknowledge the support of the Natural Sciences and Engineering Research Council of Canada (NSERC), [RGPIN-2023-03575]. Cette recherche a été financée par le Conseil de recherches en sciences naturelles et en génie du Canada (CRSNG), [RGPIN-2023-03575].

## References

1. Carroll, M.: Ejection fraction: Normal range, low range, and treatment (Nov 2021), <https://www.healthline.com/health/ejection-fraction>
2. Dai, W., Li, X., Ding, X., Cheng, K.T.: Cyclical self-supervision for semi-supervised ejection fraction prediction from echocardiogram videos. *IEEE Transactions on Medical Imaging* **42**(5), 1446–1461 (2022)
3. Fiaz, M., Heidari, M., Anwer, R.M., Cholakkal, H.: Sa2-net: Scale-aware attention network for microscopic image segmentation. *arXiv preprint arXiv:2309.16661* (2023)
4. Fraleigh, C.D., Duff, E.: Point-of-care ultrasound: An emerging clinical tool to enhance physical assessment. *The Nurse Practitioner* (2022)
5. Heidari, M., Azad, R., Kolahi, S.G., Arimond, R., Niggemeier, L., Sulaiman, A., Bozorgpour, A., Aghdam, E.K., Kazerouni, A., Hacihaliloglu, I., et al.: Enhancing efficiency in vision transformer networks: Design techniques and insights. *arXiv preprint arXiv:2403.19882* (2024)
6. Kalogeropoulos, A.P., Fonarow, G.C., Georgiopoulou, V., Burkman, G., Siwamogsatham, S., Patel, A., Li, S., Papadimitriou, L., Butler, J.: Characteristics and outcomes of adult outpatients with heart failure and improved or recovered ejection fraction. *JAMA cardiology* **1**(5), 510–518 (2016)
7. Kazemi Esfeh, M.M., Luong, C., Behnami, D., Tsang, T., Abolmaesumi, P.: A deep bayesian video analysis framework: towards a more robust estimation of ejection fraction. In: *International Conference on Medical Image Computing and Computer-Assisted Intervention*. pp. 582–590. Springer (2020)

8. Lai, S., Zhao, M., Zhao, Z., Chang, S., Yuan, X., Liu, H., Zhang, Q., Meng, G.: Echomen: Combating data imbalance in ejection fraction regression via multi-expert network. In: International Conference on Medical Image Computing and Computer-Assisted Intervention. pp. 624–633. Springer (2024)
9. Maani, F.A., Saeed, N., Matsun, A., Yaqub, M.: Corecho: Continuous representation learning for 2d+ time echocardiography analysis. In: International Conference on Medical Image Computing and Computer-Assisted Intervention. pp. 591–601. Springer (2024)
10. Mokhtari, M., Ahmadi, N., Tsang, T.S., Abolmaesumi, P., Liao, R.: Gemtrans: A general, echocardiography-based, multi-level transformer framework for cardiovascular diagnosis. In: International Workshop on Machine Learning in Medical Imaging. pp. 1–10. Springer (2023)
11. Mokhtari, M., Tsang, T., Abolmaesumi, P., Liao, R.: Echognn: explainable ejection fraction estimation with graph neural networks. In: International Conference on Medical Image Computing and Computer-Assisted Intervention. pp. 360–369. Springer (2022)
12. Muhtaseb, R., Yaqub, M.: Echocotr: Estimation of the left ventricular ejection fraction from spatiotemporal echocardiography. arXiv (2022)
13. Muhtaseb, R., Yaqub, M.: Echocotr: Estimation of the left ventricular ejection fraction from spatiotemporal echocardiography. In: International Conference on Medical Image Computing and Computer-Assisted Intervention. pp. 370–379. Springer (2022)
14. Muldoon, M., Khan, N.: Lightweight and interpretable left ventricular ejection fraction estimation using mobile u-net. IEEE ISBI (2023)
15. Ostvik, A.e.a.: Real-time automatic ejection fraction and foreshortening detection using deep learning. IEEE Transactions on Ultrasonics, Ferroelectrics, and Frequency Control (2020)
16. Ouyang, D., He, B., Ghorbani, A., Yuan, N., Ebinger, J., Langlotz, C.P., Heidenreich, P.A., Harrington, R.A., Liang, D.H., Ashley, E.A., et al.: Video-based ai for beat-to-beat assessment of cardiac function. *Nature* **580**(7802), 252–256 (2020)
17. Reynaud, H., Vlontzos, A., Hou, B., Beqiri, A., Leeson, P., Kainz, B.: Ultrasound video transformers for cardiac ejection fraction estimation. In: Medical Image Computing and Computer Assisted Intervention–MICCAI 2021: 24th International Conference, Strasbourg, France, September 27–October 1, 2021, Proceedings, Part VI 24. pp. 495–505. Springer (2021)
18. Sadegheih, Y., Bozorgpour, A., Kumari, P., Azad, R., Merhof, D.: Lhu-net: A light hybrid u-net for cost-efficient, high-performance volumetric medical image segmentation. arXiv preprint arXiv:2404.05102 (2024)
19. Selvaraju, R.R., Cogswell, M., Das, A., Vedantam, R., Parikh, D., Batra, D.: Grad-cam: Visual explanations from deep networks via gradient-based localization. In: Proceedings of the IEEE international conference on computer vision. pp. 618–626 (2017)
20. Smistad, E.e.a.: Real-time automatic ejection fraction and foreshortening detection using deep learning. IEEE Transactions on Ultrasonics, Ferroelectrics, and Frequency Control (2020)
21. Thomas, S., Cao, Q., Novikova, A., Kulikova, D., Ben-Yosef, G.: Echonarrator: Generating natural text explanations for ejection fraction predictions. arXiv (2024)
22. Thomas, S., Gilbert, A., Ben-Yosef, G.: Light-weight spatio-temporal graphs for segmentation and ejection fraction prediction in cardiac ultrasound. In: International Conference on Medical Image Computing and Computer-Assisted Intervention. pp. 380–390. Springer (2022)

23. Varudo, R., et al.: Machine learning for the real-time assessment of left ventricular ejection fraction in critically ill patients. *Critical Care* (2022)
24. Varudo, R.e.a.: Machine learning for the real-time assessment of left ventricular ejection fraction in critically ill patients. *Critical Care* (2022)
25. Yang, J., Lin, Y., Pu, B., Guo, J., Xu, X., Li, X.: Cardiacnet: Learning to reconstruct abnormalities for cardiac disease assessment from echocardiogram videos. In: *European Conference on Computer Vision*. pp. 293–311. Springer (2025)